Tellus
SERIES A
DYNAMIC
METEOROLOGY
AND OCEANOGRAPHY
PUBLISHED BY THE INTERNATIONAL METEOROLOGICAL INSTITUTE IN STOCKHOLM

Tellus (2009), 61A, 17–34
Printed in Singapore. All rights reserved

TELLUS

Numerical simulation of a mesoscale convective system over the east coast of South Africa

By R. C. BLAMEY* and C. J. C. REASON, *Department of Oceanography, University of Cape Town, Private Bag X3, Rondebosch, 7701, South Africa*

(Manuscript received 1 October 2007; in final form 11 August 2008)

ABSTRACT

Weather stations over northern KwaZulu-Natal, South Africa, recorded over 100 mm of rainfall during the night of 11–12 February 2005. This heavy rainfall was associated with a mesoscale convective system (MCS) that was initiated from small convective storms beginning early in the afternoon on 11 February 2005. An analysis of Medium Range Forecast (MRF) model output suggests that a combination of synoptic features contributed to the evolution of the system. It is likely that the high-lying topography of the eastern escarpment and high diurnal surface heating provided the trigger for the event. Although MCSs are not uncommon in this region, very little work has been done on South African cases.

The MCS is investigated with a non-hydrostatic numerical model (mesoscale model version 3; MM5) to help determine which processes were important in its initiation and development, as well as what factors contributed to the associated heavy rainfall. The model results suggest that the eastern escarpment played a key role in triggering the convective event, as well as influencing the low-level winds that advected moisture into the region. It was also apparent that the Agulhas Current played an important role in supplying moisture to fuel the extreme rainfall. The development of the MCS and the heavy nocturnal rainfall was due to a combination of the continuous moisture supply into the region, a conditionally unstable atmosphere, and uplift due to low-level convergence and the local topography.

1. Introduction

South Africa is bounded on the west by the cold upwelling Benguela Current system, and on the east, where KwaZulu-Natal (KZN) is located, by the warm Agulhas Current. Strong sea surface temperature (SST) gradients between the Agulhas Current and the ambient ocean have been shown to be important for the weather and climate of the region (Jury et al., 1993; Crimp and Mason, 1999; Reason, 2001; Rouault et al., 2002; Singleton and Reason, 2006, 2007). The South African coast is separated from an elevated plateau (approximately 1–2 km above sea level) by a well-defined escarpment that extends above 3 km in certain places within the Drakensberg Mountain Range in KZN and the Lesotho Maluti Mountains (Fig. 1). It is this escarpment that limits the low-level moisture penetration to the interior of the country from the Southwest Indian Ocean.

Most of the rainfall over the east coast and also the interior of the country is of convective origin (Tyson and Preston-Whyte, 2000). These authors suggest that the amount of convection over South Africa is determined not only by the diurnal heating cycle of the near-surface air, but also by the prevailing dynamics of particular synoptic conditions and by mesoscale and local effects. They also noted that the severe storms in the region are often the result of different forcing mechanisms ranging from the synoptic scale down to the local scale.

Severe weather experienced in South Africa includes cut-off lows (e.g. Singleton and Reason, 2006, 2007), a variety of thunderstorms, ranging from single cells storms through to the larger mesoscale convective systems (MCSs; Laing and Fritsch, 1993b; Garstang and Tyson, 2000; Tyson and Preston-Whyte, 2000), and occasionally tropical cyclones in the northeast or KZN (Dyson and van Heerden, 2001; Reason and Keibel, 2004). Although these systems may result in devastating floods and strong winds, they often provide much of the all important rainfall to semi-arid South Africa. In contrast to other areas of the world where much research has been conducted on flooding and the associated weather systems (e.g. Maddox et al., 1979; Doswell et al., 1996; Smith et al., 2001), very little has been done in South Africa on this topic.

This paper looks at a case study of an MCS that took place over northern KZN in February 2005. The term MCS is used to describe an ensemble of convective storms that satisfy certain spatial and temporal criteria. Due to the variety of MCSs, they can be broadly defined as a long-lived (≥3 h) cumulonimbus

*Corresponding author.
e-mail: ross.blamey@uct.ac.za
DOI: 10.1111/j.1600-0870.2008.00366.x

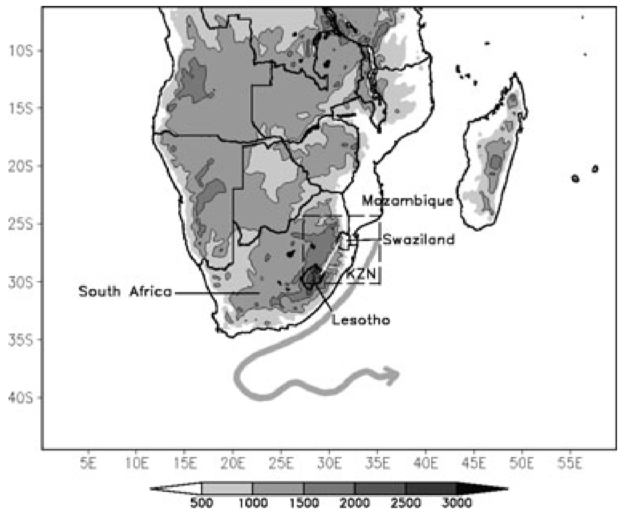

Fig. 1. Topography of southern Africa from the 5-min resolution USGS data set (shaded). The white line denotes the approximate location of the eastern escarpment, including the Drakensberg Mountain Range. The grey line shows the approximate location of the Agulhas Current and its retroflection back into the South Indian Ocean. Also shown is the position of the nested domain used for the model simulations, as well as the countries referred to in the text and the location of KwaZulu-Natal (KZN).

cloud system that contains a nearby precipitation area of roughly 100 km or more in at least one direction (Parker and Johnson, 2000; Houze, 2004). The largest of such systems is the quasi-circular 'mesoscale convective complex' (MCC), defined by Maddox (1980) to fall within the meso-α scale (Orlanski, 1975). Some of the requirements which define the different types of MCS are based on cloud top temperature, size, duration and eccentricity/shape (e.g. Maddox, 1980).

MCSs have been documented in many regions, including parts of North and South America, Europe, Asia, Australia and Africa (Maddox, 1980; Velasco and Fritsch, 1987; Miller and Fritsch, 1991; Laing and Fritsch, 1993a, 1993b, 1997, 2000; Anderson and Arritt, 2001; García-Herrera et al., 2005 and others). However, most of this research on these weather systems has been conducted outside Africa. The limited research that has been done on African systems has mainly focused on systems in the Sahel Region (e.g. Laurent et al., 1998; Laing et al., 1999; Mathon et al., 2002). Thus, an important aspect of the ongoing research is to examine MCSs over southern Africa and their associated impacts.

Forecasting MCSs over southern Africa remains a difficult task due to insufficient radar and satellite observations, radiosonde data and limited modelling capacity. Despite the lack of observations, numerical modelling may play an important role in advancing our understanding of extreme events in the region. Thus, we conduct a numerical study on one such event to obtain a better understanding of the processes that governed the development and life cycle of the system, as well as its associated heavy rainfall. As far as we know, this study is the first attempt to model an MCS over South Africa.

Following this introduction, Section 2 provides an overview of the event as well as the synoptic conditions. The numerical model is discussed in Section 3. This is followed by an analysis of results from the simulations in Section 4. The final section contains the conclusions.

2. Overview of the event and synoptic setting

This MCS is of interest due to the large amounts of rainfall it produced, particularly along the north coast of KZN (Fig. 2). Rain gauges along the northern coastline recorded over 100 mm during the night/morning of the 11–12 February 2005, with the maximum being 119 mm. Swaziland, to the north of KZN, also received heavy rainfall during the event, with the maximum being 101 mm. Note that rainfall data were not accessible for Mozambique, and thus Fig. 2 does not show the northern limit of the rainfall distribution. The location of the heavy rainfall over the east coast is reflected in the Tropical Rainfall Measuring Mission (TRMM) rainfall (not shown), which also indicated that heavy rainfall took place just off the east coast over the Agulhas Current. This single event had a large influence on the February rainfall total, leading to some regions having above average rainfall for the month or for the core summer rainy season (December–February) as a whole. Rainfall data from the Richards Bay and Cape St. Lucia stations showed that this event contributed approximately 20% to the DJF rainfall total at both places.

In terms of life cycle, the system appeared to follow the general pattern identified for MCCs over southern Africa (Laing and Fritsch, 1993b). Sequences of infrared satellite images reveal that the large cloud system developed over the east coast

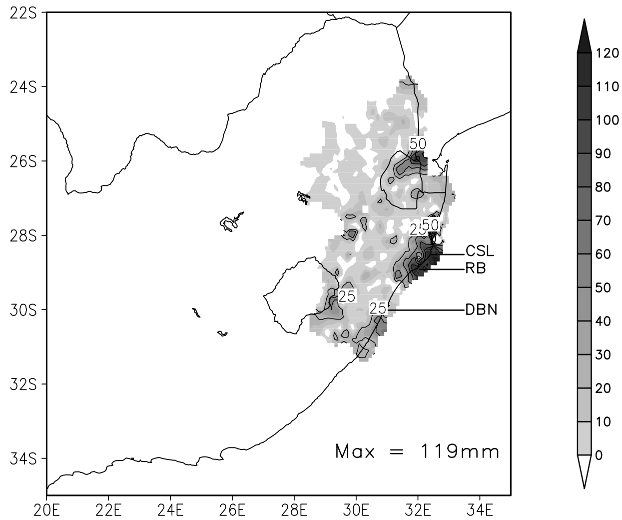

Fig. 2. Map showing rainfall over the 11–12 February 2005 from the SAWS station data. Place names referred to in the text are: DBN—Durban, RB—Richards Bay and CSL—Cape St. Lucia.

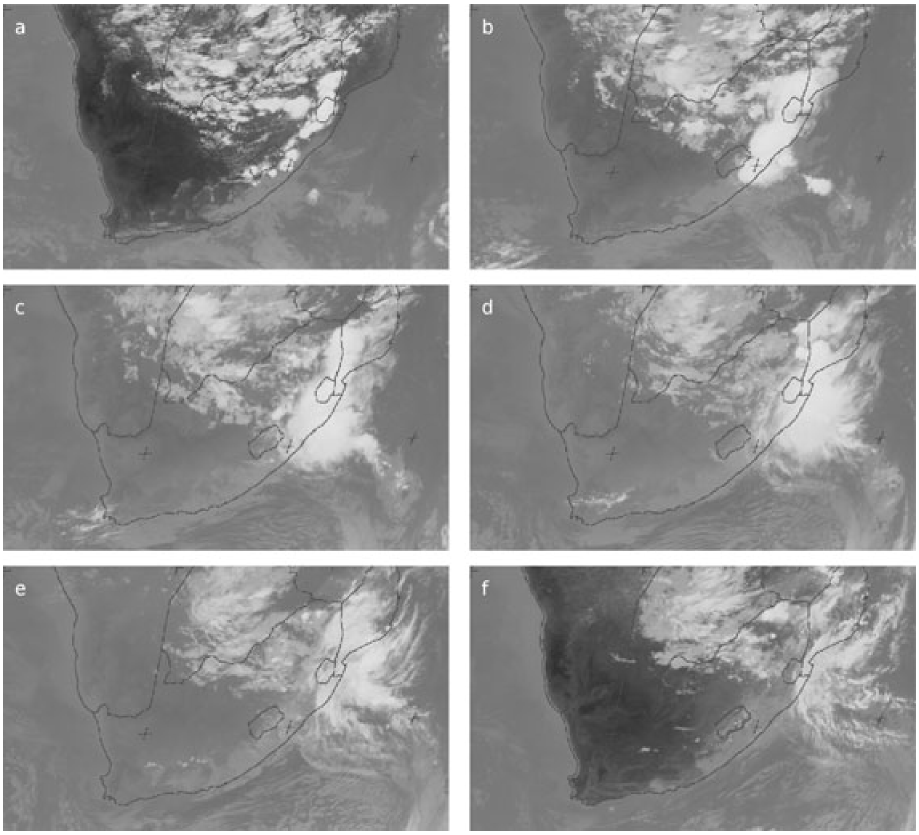

Fig. 3. Meteosat infrared satellite images at 4 h intervals (from left-hand side to right-hand side) starting at (a) 1342 UTC 11 February (top left-hand side) through to (f) 0942 UTC 12 February (bottom right-hand). The three crosses in the figures represent 30°S, 20°E (far left-hand side), 30°S, 30°E (middle) and 30°S, 40°E (far right-hand side).

of South Africa during the afternoon and night (local time) of 11–12 February (Fig. 3). The MCS developed from a few single cell storms along the Drakensberg Mountains, which then merged and developed as a single cloud system. The merging or interaction of individual storms into one big system is a common feature found in the development of MCCs (Maddox et al., 1986). As the system grew in strength, it propagated eastwards towards the northern Agulhas Current. From the satellite images, it appears that the system started to obtain MCS status around 1600–1700 UTC (UTC = LST – 2) 11 February and lasted approximately 10 h, until it started to decay just after 0200 UTC the next morning. The system appeared to reach maximum extent between 2200 and 0000 UTC 11 February. The tendency of these systems to occur mainly at night is believed to be related to radiation and latent heating processes (Cotton, 2000).

Initially, the system assumed a linear form, but later in its life cycle, became more circular in appearance. As mentioned previously, the shape of the system is usually one of the methods applied to help determine the type of MCS. Linear MCSs are more commonly referred to as squall lines, while quasi-circular systems are usually referred to as MCCs. However, in this case, the system did not reach MCC status as defined by Maddox (1980) since it did not contain the correct eccentricity for a long enough duration although it did manage to attain the required cloud top temperatures (not shown) and size.

National Center for Environmental Prediction (NCEP) Medium Range Forecast (MRF) analysis data (Kanamitsu, 1989; Kalnay et al., 1990; Kanamitsu et al., 1991) reveal that during the event, key synoptic features were present over southern Africa and the surrounding oceans during the event. At 1200 UTC 10 February, a weak cold front was located to the south of the country, with an anticyclone approaching from the west, and a trough was present over interior South Africa (not shown). Another anticyclone was situated in the Southwest Indian Ocean, with a low-pressure sitting between the country and this anticyclone. These synoptic conditions resulted in easterly/northeasterly low-level winds transporting moist tropical air along the KZN coastline.

By 0000 UTC 11 February, the South Atlantic anticyclone began to ridge south of the country, while the weak cold front had propagated towards the east (not shown). A ridging anticyclone, which is a common occurrence during the summer rainfall season and has a peak in frequency during the months of October and February, is known to produce widespread rainfall over the eastern parts of southern Africa (Tyson and Preston-Whyte, 2000). Analysis of the 500 hPa heights showed that between

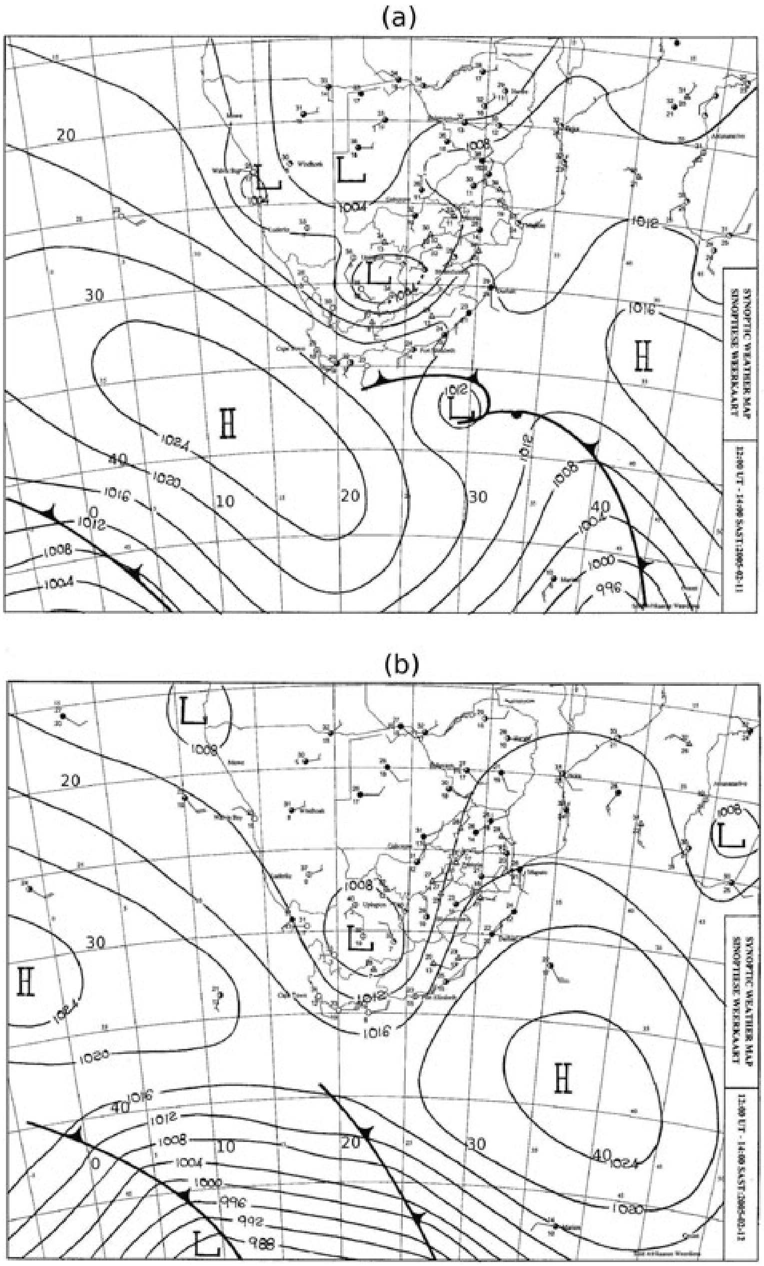

Fig. 4. South African Weather Service synoptic charts for the (a) 11 February 2005 and (b) 12 February 2005 (all at 1200 UTC).

0000 and 1200 UTC 11 February a weak westerly wave passed over the southern parts of the country (not shown). A westerly wave at mid-levels has been found to play an important role in initiating MCSs in the U.S. (e.g. Maddox, 1983, Cotton et al., 1989), but in this case it did not appear to have such an influence.

At 1200 UTC 11 February, the ridging anticyclone was situated to the south of the country (Fig. 4). Associated with this system were moderate onshore winds onto the east coast (Figs. 5a–c). Moisture from the Southwest Indian Ocean has also been known to fuel heavy rainfall events along the Eastern Cape (e.g. Crimp and Masson, 1999; Rouault et al., 2002; Singleton and Reason, 2006). These low-level winds supply significant moisture into the region due to their passage across the warm SST of the Agulhas Current. Moisture flux diagrams reveal that a relatively large quantity of moisture was advected into the storm region at the 1000 hPa level (Fig. 6). These moisture flux values, which are calculated from specific humidity and wind data taken from the National Center for Environmental Prediction/National Center for Atmospheric Research (NCEP/NCAR) re-analysis data (Kalnay et al., 1996), indicate that the largest amount of moisture was advected into the region during the night of 11–12 February (140–180 g kg^{-1} m s^{-1} between 1800 and 0000 UTC 11–12 February) consistent with the heavy rainfall at this time.

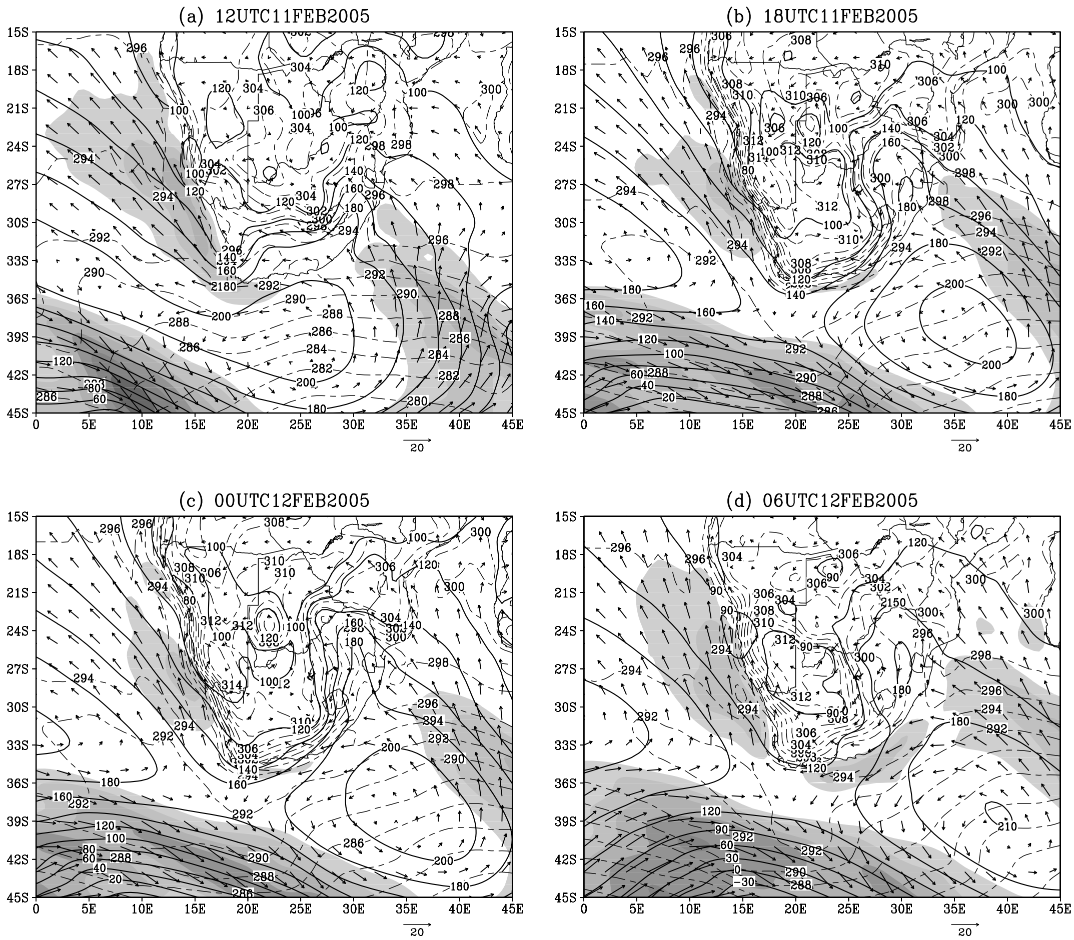

Fig. 5. Temperature (dashed contours; interval 2°K), geopotential height (thick contours; interval 20 m), wind speed vectors (with a vector scale in m s^{-1} given at the bottom of the panels) and speeds greater than 10 m s^{-1} shaded at the 1000 hPa level, derived from the MRF model. Starting at (a) 1200 UTC 11 February and ending at (d) 0600 UTC 12 February, at 6-hourly intervals.

A surface interior trough in the easterly flow over inland South Africa (Figs. 4 and 5), is also a favourable mechanism for the development of convective rainfall. This semi-stationary heat low is often associated with low-level convergence and upper-level divergence to the east of the surface trough, leading to rainfall over eastern South Africa (Tyson and Preston-Whyte, 2000). At 1200 UTC 11 February, there was considerable moisture convergence along the eastern escarpment, as well as over the coastal regions (Fig. 6). By 0000 UTC 12 February, the most intense moisture convergence was located along the northeastern parts of KZN as well as the interior. The maximum convergence values along the northern KZN region were consistent with an increase of rainfall in this region.

Radiosonde data are sparse in Africa and are only routinely available for some South African stations. The closest radiosonde station to this event is Durban, approximately 250–300 km to the southeast of where the storm initiated and about 200 km south of the region containing the heaviest rainfall. From the available soundings (not shown), it was evident that at 0900 UTC 11 February, near-surface conditions were hot and humid, while above this layer, the atmosphere was cooler and close to saturation between the 950 and the 800 hPa levels. Another feature was the presence of a low-level inversion (approximately at the 750 hPa level). This pattern of warm, moist air overlain by cool, drier air is conducive to the development of convective events. The convective available potential energy (CAPE), which may be used as an indicator for the likelihood of deep convection, reached 2896 J kg^{-1} at Durban at 0900 UTC 11 February. This reasonably high CAPE value was likely due to the humid air in the lower levels, with the environmental temperatures dropping above the 750 hPa level.

The MCS began to decay during the morning of 12 February between 0000 and 0600 UTC (Fig. 3), when the synoptic conditions no longer provided suitable conditions to sustain convection. The ridging high-pressure system shifted further eastwards, resulting in changes in the low-level wind patterns. As a result, there was also a decrease in the low-level moisture feeding the system (Fig. 6). The changes in the wind field at lower levels

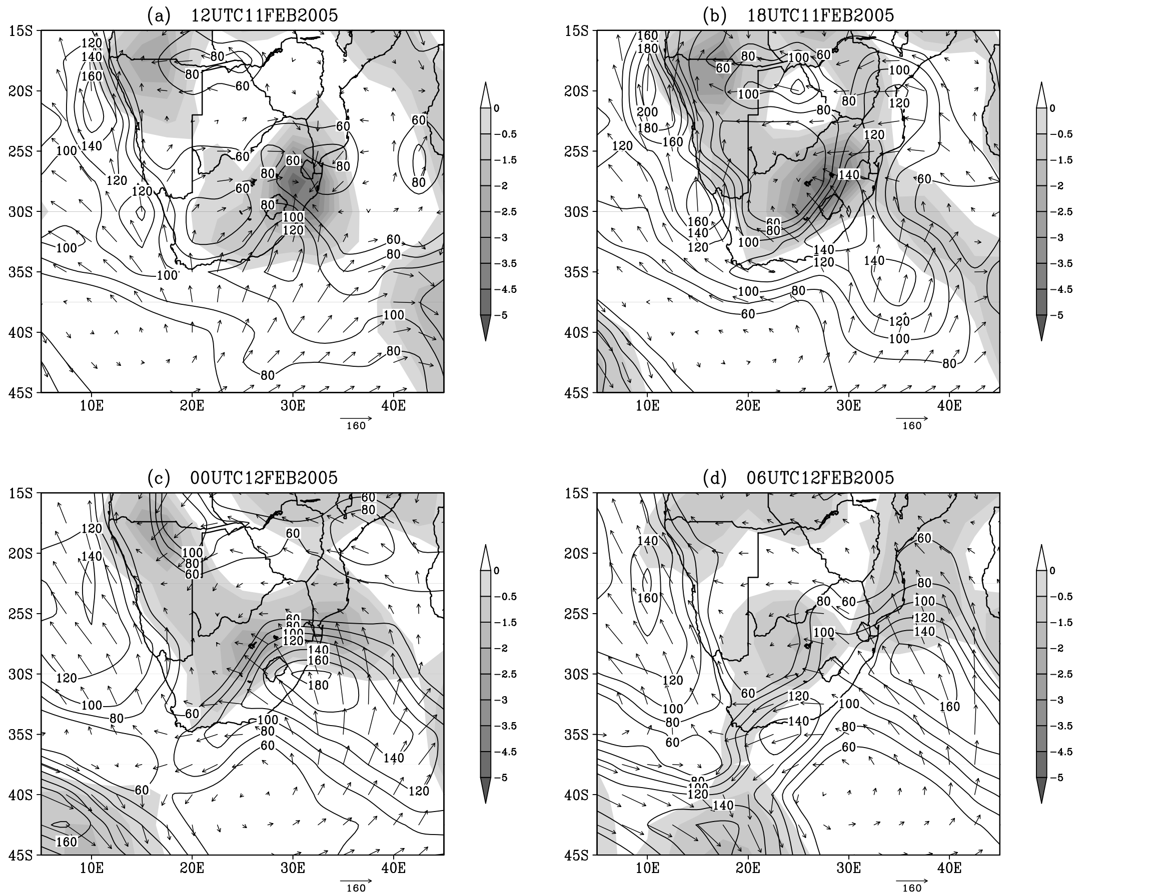

Fig. 6. National Center for Environmental Prediction 6-hourly moisture flux values (contour; interval 20 g kg^{-1} m s^{-1}), moisture flux vectors (with a vector scale in g kg^{-1} m s^{-1} given at the bottom of the panels) and moisture convergence (shaded; interval 0.5 g kg^{-1} s^{-1}) at the 1000 hPa level. Note that divergence has been omitted for clarity.

also resulted in moisture convergence in the region being replaced by moisture divergence. The interior trough had also filled from 1004 to 1008 hPa (not shown). By this time, the weak westerly wave in the mid-levels had also propagated eastwards towards the Indian Ocean. As a result, unfavourable conditions for convection now existed, leading to the decay of the system.

3. Model description and experiments

The model used was the non-hydrostatic fifth generation mesoscale model version 3 (MM5; Dudhia, 1993; Grell et al., 1994). This mesoscale model has been used to research MCS in many parts of the world, including the U.S., Africa, Europe and parts of Asia (e.g. Tucker and Crook, 1999; Chen et al., 2000; Romero et al., 2000; Xu et al., 2001 and many others), but not to date over South Africa.

In our configuration, we used 23 sigma levels from the surface up to 100 hPa, and two domains with two-way nesting. The coarse domain, at 18 km resolution, contains 271 × 370 gridpoints centred at 20°S, 30°E. The fine domain, at 6 km resolution, consists of 112 × 148 gridpoints (Fig. 1). Topography for each grid was taken from the U.S. Geological Survey (USGS) 5 and 2-min resolution data set, respectively.

The planetary boundary layer physics was parametrized using the MRF scheme (Hong and Pan, 1996) while land surface temperature and moisture over land were calculated using the five-layer soil model. Cloud cover is taken into account when calculating surface fluxes, as well as atmospheric temperature tendencies caused by long-wave and short-wave radiation components. MM5, like most models, uses a hybrid precipitation approach, with both an explicit moisture scheme and a cumulus parametrization scheme. An explicit precipitation scheme is used on the 6 km grid, while the Grell cumulus scheme (Grell et al., 1994) is used on the coarse domain. The Reisner explicit microphysics parametrization (Reisner et al., 1998) is used. In this scheme, five prognostic equations are used for water vapour, cloud water, rainwater, cloud ice and snow. It includes the effects of evaporation, condensation, hydrostatic water loading, melting, freezing, deposition, sublimation and supercooled liquid water.

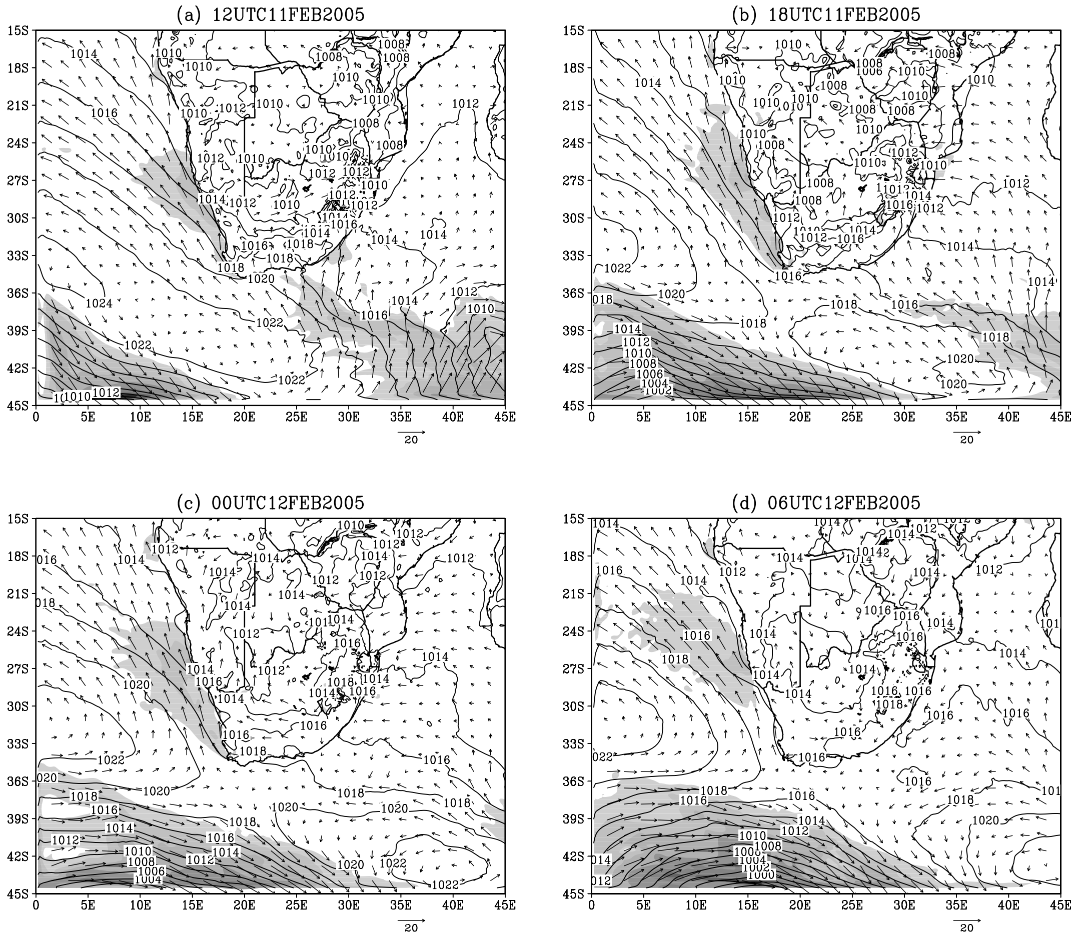

Fig. 7. Mean sea level pressure (black contours; interval 2 mb), wind speed vectors (with a vector scale in m s^{-1} given at the bottom of the panels) and speeds greater than 10 m s^{-1} shaded at the 0.995 sigma level, derived from the control simulation. At 6-hourly intervals, starting at (a) 1200 UTC 11 February and ending at (d) 0600 UTC 12 February.

Initial and boundary conditions were obtained by horizontally interpolating $1^\circ \times 1^\circ$ resolution MRF analysis data to the MM5 grid and then vertically interpolating them to the MM5 sigma levels. The SST used is taken from the 1° resolution weekly average version 2 of the NOAA Optimum Interpolation SST (OISST; Reynolds et al., 2002). These boundary conditions from the MRF model were imposed every 6 h for the outer grid, while for the nested grid, boundary conditions were applied from the mother grid at each time step with two-way nesting. The model was integrated for 72 h from 0000 UTC 10 February 2005.

4. Numerical model analysis

4.1. Model validation for synoptic features

Initializing the model at 0000 UTC 10 February 2005 was found by trial and error to produce the best results in terms of storm development, life cycle and location. To validate the simulation, the model low- and mid-level circulations are compared with the South African Weather Service (SAWS) surface and 500 hPa synoptic charts, station data and QuikSCAT satellite wind data for the ocean.

Figure 7 shows mean sea level pressure (SLP) and areas of strong wind ($>$10ms^{-1}) at the lowest level from the control simulation. As found in the MRF analysis (Fig. 5) and SAWS surface synoptic charts (Fig. 4), the propagation of the ridging anticyclone to the south of the country in the model appears to be an influential feature during the event. This synoptic feature was located to the southwest of the country at 0600 UTC 11 February 2005 and then propagated to the south of South Africa by 1200 UTC. By 0600 UTC 12 February, this model feature had then propagated out into the Southwest Indian Ocean consistent with observations. The ridging anticyclone played an important role in supplying the onshore winds into the east coast, as discussed below. Figure 7 also reveals the presence of an interior trough during the event. This inland trough appears weaker (1010 hPa) in the model compared to that found in the SAWS synoptic charts (1004 hPa; Fig. 4) at the same time. However, later that afternoon, the trough did strengthen with the central pressure decreasing to 1008 hPa.

At the 500 hPa level, the MM5 simulated synoptic pattern also appeared to be consistent with that of the MRF analysis (not shown). The eastward propagation of a westerly wave at this level was found in the MRF analysis data (not shown) and it is also apparent in the model. The model is successful in simulating the timing of this westerly wave compared to the MRF analysis and SAWS 500 hPa charts (not shown). The position and strength of the 200 hPa level jet in the model also compared favourably with the 200 hPa MRF analysis (not shown).

The low-level circulation in the control run compared favourably with SAWS synoptic charts (Fig. 4) and SAWS station data (not shown). Low-level onshore flow onto the east coast with associated advection of moisture was important for the evolution of the MCS. At 0600 UTC 11 February, northeasterlies dominated the lower model levels along the east coast of South Africa, which then veered as the day progressed, becoming southeasterlies by 1200 UTC 11 February. As the ridging anticyclone propagated out into the Southwest Indian Ocean, the wind pattern shifted and returned to northeasterlies by 0600 UTC 12 February. However, when compared to the MRF analysis, it appears the control run captures the wind direction off the east coast correctly, but slightly underestimates its strength. Over the ocean, the model winds are also weaker than those derived from QuikSCAT (not shown). These weaker winds found in the model simulation could be associated with the slightly weaker pressure gradient situated to the southeast of the country in the model.

Overall, simulation of the synoptic features compares favourably to those observed in the MRF model analysis, QuikSCAT winds, and SAWS synoptic charts and station data. It was evident that the model was able to simulate the evolution of the synoptic features associated with the development and life cycle of the convective event. Although there are some subtle differences between the control run and MRF data, the model appears to perform sufficiently well to be used to better understand the evolution of the event.

4.2. *Storm development, precipitation and moisture transport*

Several variables have been used as proxies for MCS detection. For example, Bernardet et al. (2000) used vertical velocity, Chen et al. (2000) used rainwater, while Xu et al. (2001) used SLP fields. Outgoing long-wave radiation (OLR) is also used as a proxy for precipitation or at least convective cloud cover (e.g. Xie and Arkin, 1998). In our study, it was evident that areas of low OLR values (i.e. substantial convective cloud cover) coincided with high values of precipitable water (>4.5 cm; not shown), suggesting that OLR values are a suitable proxy.

The initiation region of the simulated system and its subsequent evolution (not shown) appears similar to that observed in the satellite images shown in Fig. 3. At first, a few single cell systems developed along the eastern escarpment in the mid-afternoon, which merged to form one system during the evening. The simulated system gained its maximum size at about 2300 UTC and then began to decay. However, a few noticeable differences between the OLR figures and the satellite observations are apparent. The shape of the system differs slightly from that of the observations, since the latter retained a more linear shape for longer than in the model. In addition, the observed system initiated slightly earlier than the model and also lasted longer.

Figure 8a indicates that the model precipitation has a similar spatial distribution to the observed (Fig. 2) and TRMM rainfall, although it overestimates the amount along the north coast as well as over the adjacent Agulhas Current. Excess precipitation is also simulated in the high-lying topography regions of the northeast escarpment. Too little model precipitation occurred over the Cape St. Lucia region. Error in simulated precipitation appears to be a common problem in mesoscale modelling, and may be related to the parametrizations of convection and cloud microphysics (e.g. Kuo et al., 1997; Wang and Seaman, 1997).

South African Weather Service station data indicated that most of the intense precipitation took place along the north coast of KZN between 2200 and 0200 UTC 11–12 February. The model simulation appeared to follow a similar pattern with the heavy nocturnal rainfall along the north coast (not shown). Initially, precipitation occurred along the eastern escarpment when the system began to develop. Precipitation then spread eastwards as the system propagated towards the coastline.

During the period of heavy rainfall, it was evident that a strong easterly influx of moisture was impinging on the KZN coastline, while low-level moisture convergence was also present (Fig. 9a). The atmosphere overlying the east coast appeared to be convectively unstable at the time, calculated from the difference in equivalent potential temperature between the 0.995 and the 0.525 sigma levels (Fig. 9b). The instability in the region was likely due to the low-level advection of warm, moist air that originated from over the Agulhas Current, where fairly large surface latent heat fluxes were evident (Fig. 9c).

A common feature in the development of MCSs elsewhere in the world that appears to be absent here in both the MRF and model data is that of a low-level jet (LLJ). In this case, the presence of a LLJ was judged on wind speeds exceeding 10 ms^{-1}, as well as changes in wind speed with height in the coastal region. At 1200 UTC 11 February, there was a moderate southeasterly wind impacting on the coast (Fig. 7a), which helped supply moisture into the region. The timing of the heavy precipitation along the north coast appeared to coincide with the onset of moderate easterly onshore winds (surface to 850 hPa). These winds weakened a few hours later and shifted further offshore, thus reducing the amount of moisture into the region.

Moisture advection into the heavy rainfall region occurred from the surface to about 700 hPa due to mesoscale anticyclonic circulation evident in the lower atmosphere along the east coast

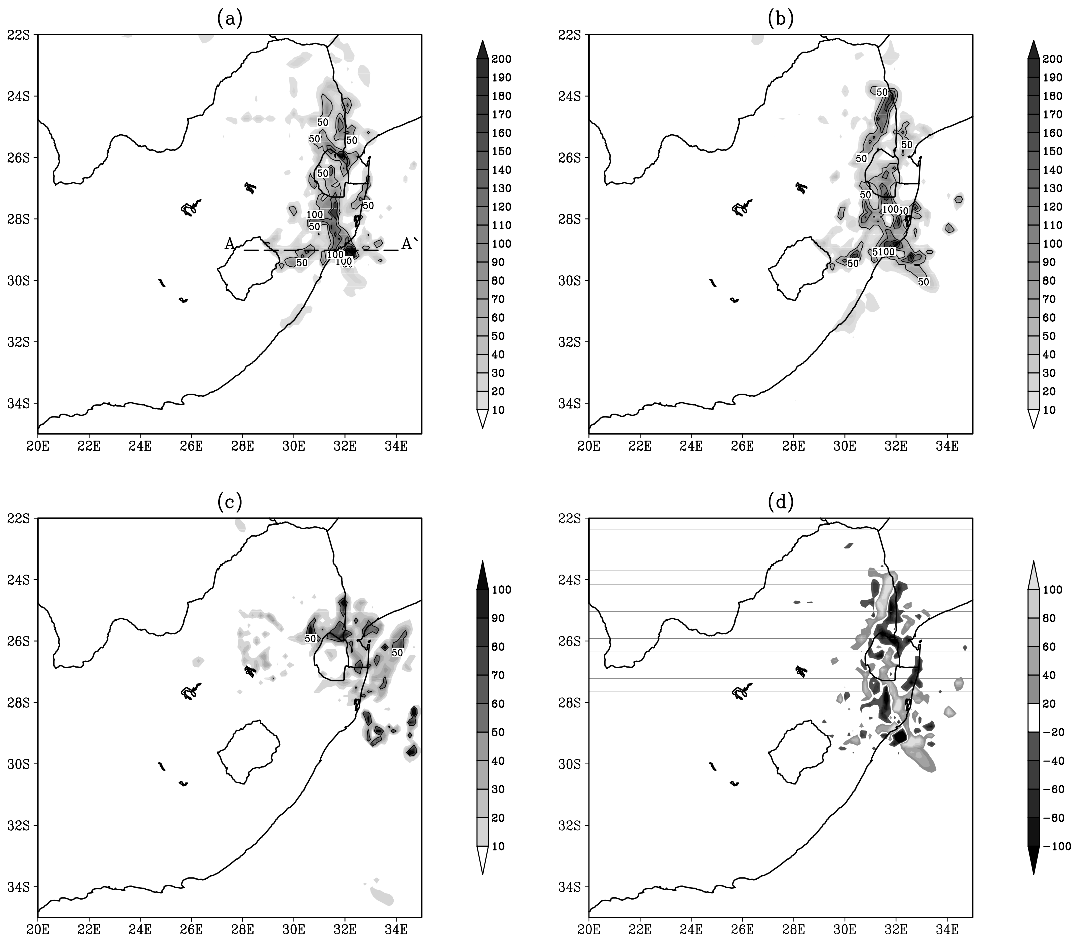

Fig. 8. Mesoscale model version 3 simulated precipitation (mm) for 11–12 February 2005 for (a) the control, (b) 'exSST', (c) 'exTOPO' model runs and (d) difference in rainfall between 'exSST' and the control.

(Fig. 9d), which propagated from the southwest. By the late morning on 12 February, this feature had propagated further off the east coast and had weakened, resulting in less moisture advected into the region. There does not appear to be any signal of this feature in the MRF or QuikSCAT data, which could possibly be due to the substantially lower resolution of these data compared to the 6 km of the nested model grid.

To obtain a better idea of the moisture transport into the region of the storm initiation and life cycle, backward trajectories were computed with the hourly MM5 model output. The trajectories were calculated using the Hybrid Single Particle Lagrangian Integrated Trajectory model (HYSPLIT4; Draxler and Hess, 1997) developed by the Atmosphere Resources Laboratory (ARL) at NOAA. Backward trajectories were computed for regions near the storm initiation and along the coastal regions where maximum precipitation occurred. A total of four different parcels were released backwards, corresponding to the lower, mid- and upper levels.

Figure 10 shows backward trajectories from one of the heavy rainfall regions. The low-level air parcels originated from the northeast and then travelled across the warm Agulhas Current along the east coast before heading inland towards the escarpment. Air parcels at mid-levels also originated over the ocean, whereas the air at upper levels came from the drier interior (Fig. 10). Analysis of 18 km weekly interpolated Advanced Very High Resolution Radiometer (AVHRR) multichannel SST data (MCSST; http://poet.jpl.nasa.gov), indicated that anomalously warm waters occurred off the east coast, thus enhancing the moisture flux towards the storm. The trajectory analysis indicated that the moist low-level airmass in the storm region was overlain by cool, drier air originating from the South Atlantic (not shown) leading to convective instability over KZN.

These results from the backward trajectories are consistent with previous research, which has shown that moisture sources for the South African summer precipitation region include the neighbouring tropical oceans (D'Abreton and Lindesay, 1995; Cook et al., 2004), tropical Africa (D'Abreton and Lindesay, 1993; Cook et al., 2004) and the Agulhas Current region off the south coast (Jury et al., 1993; Rouault et al., 2002; Singleton and Reason, 2006, 2007). Cook et al. (2004) found that most

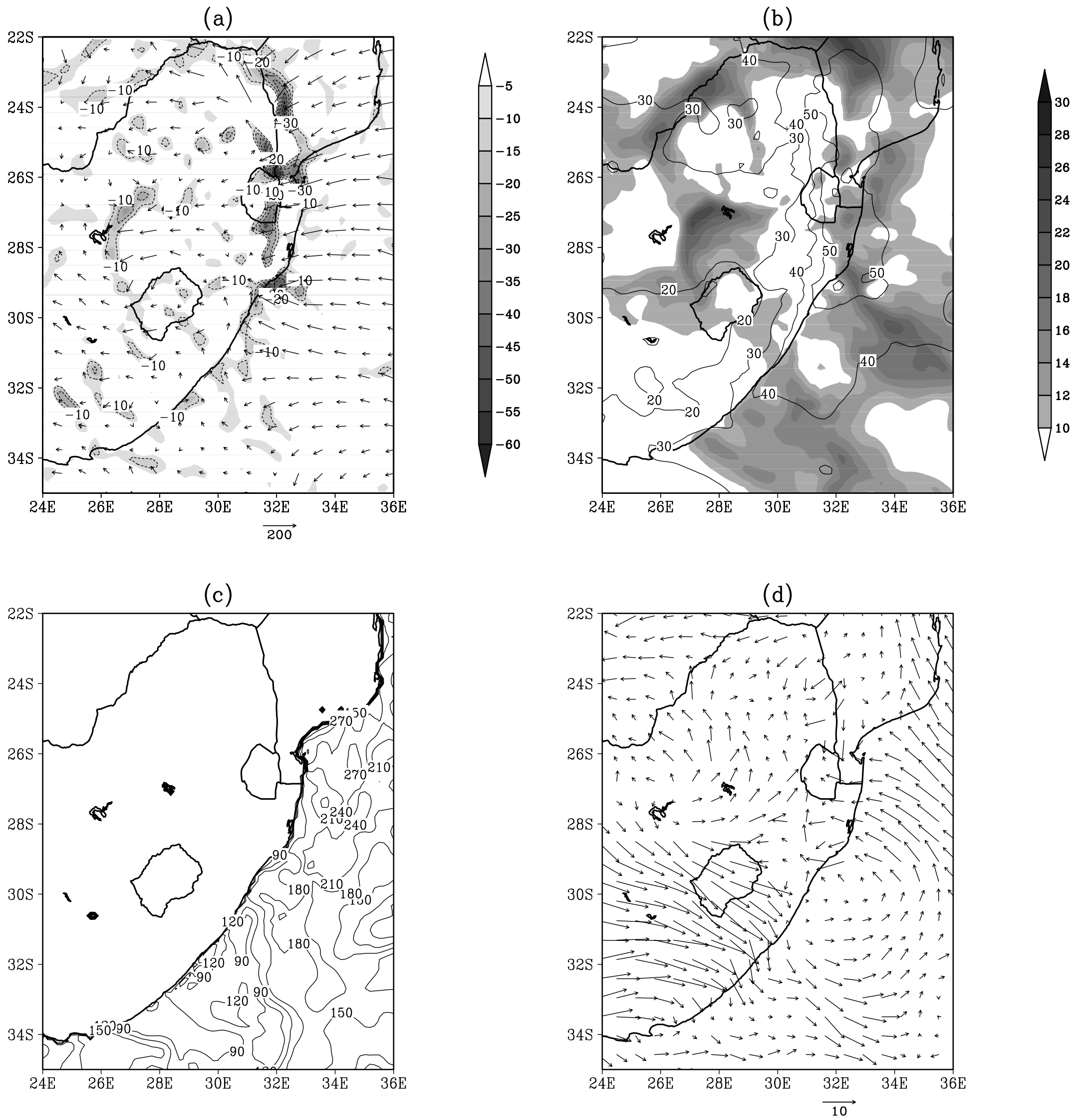

Fig. 9. Output from the control at 2300 UTC 11 February 2005. (a) 0.995 moisture flux (vector scale in g kg^{-1} m s^{-1} given at the bottom) and moisture flux convergence (shaded 5 g kg^{-1} s^{-1} interval), (b) precipitable water at 0.995 sigma level (contour interval 10 mm) and convective instability taken as difference between equivalent potential temperature between 0.995 and 0.525 sigma level (shaded 2 K interval), (c) surface latent heat flux, contour interval 30 W m^{-2} and (d) wind vectors at the 0.725 sigma level (vector scale in m s^{-1} given at the bottom).

wet spells in the summer South African precipitation region coincided with increased influx of moisture from the Southwest Indian Ocean and convergence over the precipitation region.

4.3. *Vertical structure of the troposphere during the event*

To get a better understanding of the conditions through the troposphere during the heavy precipitation event, east-west vertical cross-sections are produced (A–A′ in Fig. 8a). At times of maximum hourly precipitation, the region experienced onshore winds and strong uplift (Fig. 11a). This uplift of moist air extends from the boundary layer up to 300 or 200 hPa, particularly from late afternoon on 11 February. Further inland, strong uplift began around 1500 UTC 11 February. The coastal region was characterized by ongoing uplift due to the inflow of low-level moisture and the coastal topography.

Low-level convergence and mid-upper-level divergence were prominent over the coastal region aiding the development of heavy precipitation (Fig. 11b). This pattern resulted in the intensification of the MCS due to the low-level convergence forcing uplift and then mid-upper-level divergence evacuating this air, allowing more moist air to rise. Ascending moist columns extended to 400 or 300 hPa during the periods of strong uplift

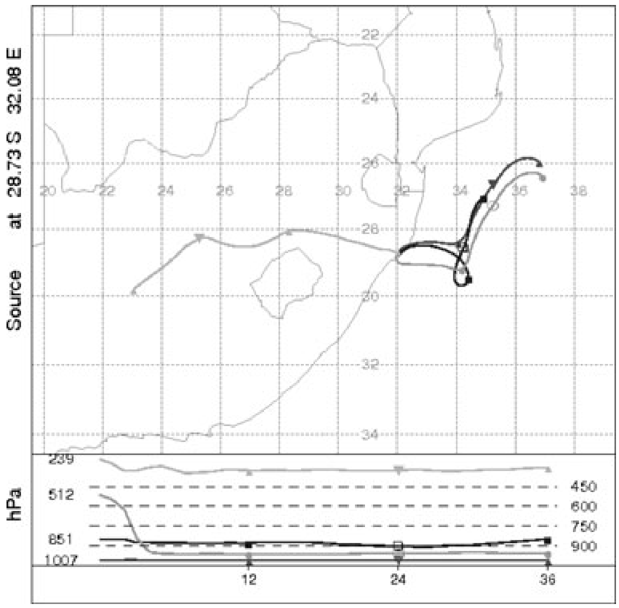

Fig. 10. Thirty-six hour backward trajectories of air parcels released at Richards Bay station (28.73°S; 32.08°E) at 0000 UTC 12 February. The location coordinates are found on the left-hand side of the image, while the altitude of the different air parcels is found in the bottom panel.

(Fig. 11c), consistent with heavy rainfall production. This structure persisted through the night of 11–12 February, but began to weaken in the early morning of 12 February.

Vertical plots of equivalent potential temperature (θ_e; Fig. 11c) show a thermal ridge located near the maximum rainwater mixing ratio. When the cross-section was extended further east (not shown), a steep vertical gradient in the equivalent potential temperature was also present during the heavy precipitation periods during 11–12 February 2005. These steep vertical gradients of equivalent potential temperature suggest that moisture was transported into the region from the surrounding ocean (Juneng et al., 2007).

Plots of convective instability suggested that during the event, the atmosphere was convectively unstable, particularly along the northern KZN coast in the afternoon and evening. The convective instability figures are supported by the soundings from the model for the Richards Bay and Durban region (both not shown). At Richards Bay, the atmosphere was close to saturation over most of the profile whereas further south at Durban, near-saturated conditions at low levels were overlain by a drier atmosphere aloft.

Doswell et al. (1996) suggest that for deep convection to occur, three criteria are required, namely the presence of low-level convergence, upward motion and instability. The control simulation suggests that all three of these criteria were satisfied over the northeastern KZN region. Thus, the heavy nocturnal rainfall over coastal KZN resulted from prolonged conditions favouring the development of deep convection.

4.4. *Sensitivity tests: SST and topography*

The simulation suggests that both regional topography and SST played a significant role in the life cycle of the system. Topography appeared to have had an influence in the initiation of the system, whereas the low-level flow across the warm Agulhas Current led to more moisture input into the storm. Thus, two other model runs were conducted where (1) a higher resolution SST data set was used (exSST) and (2) the topography was reduced by 75% (exTOPO) compared to the control.

4.4.1. SST resolution. The horizontal resolution of the SST used in the control is 1°, which is too low to resolve the core of the Agulhas Current as well as the steep SST gradients. Rouault et al. (2003) have shown that the core of the current leads to observed surface latent and sensible heat fluxes that are much larger than those estimated by NCEP and ECMWF using coarser resolution SST. In 'exSST', AVHRR 18 km weekly interpolated MCSST data were used to force the model.

Figures 8b and d indicate that the higher resolution SST forcing 'exSST' leads to considerably more precipitation than the control over the Agulhas Current region, as well as some parts of northeastern South Africa and Swaziland. The OLR distribution in 'exSST' (not shown) shows that the MCS evolves a very similar shape and track as in the control run. However, in 'exSST', the MCS was larger on its poleward side in the latter stages of the run when the MCS was located over the Agulhas Current region, since SST gradients there are enhanced. This increased development on its poleward side, which is similar to that found in the satellite data, could explain the greater precipitation found in 'exSST' off the east coast.

The low-level synoptic conditions in the 'exSST' simulation were very similar to that found in the control run. The direction and magnitude of the winds at the lowest level in 'exSST' were similar to those in the control, which showed the continuous onshore flow along the east coast. It is likely that these onshore winds in 'exSST' advected more moisture into the region due to the higher resolution SST data. There was also evidence of a weak easterly LLJ developing during the night, which was not identified in the control run. Vertical cross-sections of wind speed and zonal wind off the east coast suggested that the onshore winds in the lower levels were a dominant feature through much of the event in 'exSST'.

Moisture flux values from 'exSST' indicated that large quantities of low-level moisture were advected into the region during the heavy rainfall (Fig. 12a). Southeasterly moisture advection was dominant during the afternoon of 11 February, but was then replaced by easterly advection later that day. In addition, stronger low-level moisture convergence took place over the east coast in 'exSST' (Fig. 12a) compared to the control. The surface latent heat fluxes over the northern Agulhas Current were greater in

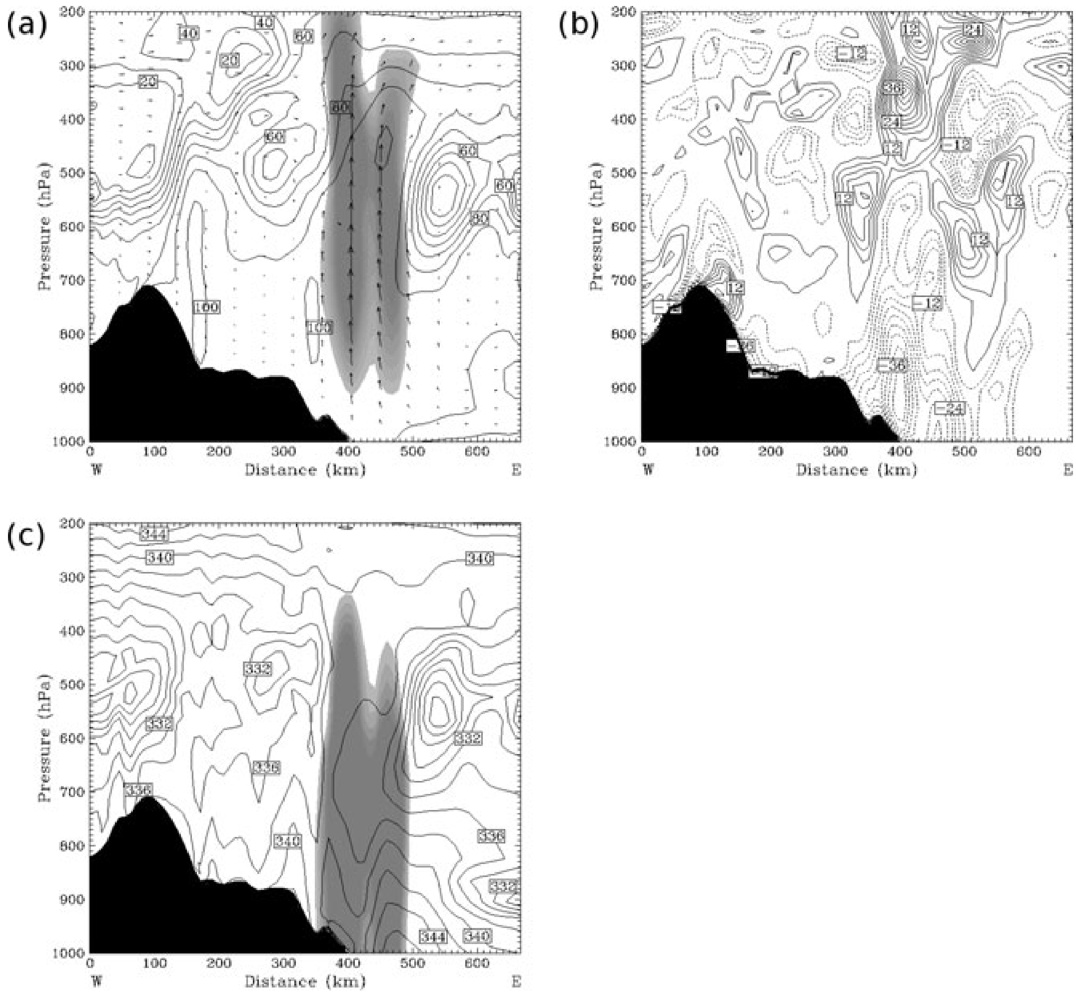

Fig. 11. Vertical cross-sections taken at 2300 (UTC) along A–A′ (see Fig. 8a) in the control simulation of (a) wind vectors, vertical velocity greater than 40 cm s^{-1} (shaded) and relative humidity (contours with an interval of 10%), (b) divergence (interval 4 s^{-1}) and (c) equivalent potential temperature (interval 2 K) and rainwater mixing ratio greater than 0.4 g kg^{-1} (shaded).

'exSST' (Fig. 12c) consistent with the larger values of low-level moisture convergence experienced in the region.

The convective instability (Fig. 12b) at the time of heaviest rainfall was also very similar to that found in the control run. Model soundings taken for Durban and Richards Bay (both not shown) suggest that the lower atmosphere was near saturation during the afternoon and night. Figure 12b indicates that the area of precipitable water content with values exceeding 50 mm over the KZN region and neighbouring areas was slightly greater in 'exSST' than in the control run.

Figure 13 shows vertical cross-sections taken through one of the heavy rainfall regions in 'exSST'. It is apparent that similar features that resulted in the heavy rainfall in the control are present in 'exSST'. These factors include strong low-level convergence and mid-level divergence (Fig. 13b), a high moisture content, strong uplift (Fig. 13a) and persistent onshore flow in the lower levels.

It seems that the increase in SST resolution in 'exSST' led to more moisture being transported into the east coast region, but to what extent this influenced the extreme precipitation pattern is not so obvious. It was also apparent that when the MCS was positioned over the Agulhas Current region in 'exSST', it took longer to dissipate. This result suggests that fluxes over this warm current and the close proximity of moisture may have strengthened the system. Note that although the MCSST data contain a fairly high spatial resolution, temporally, they still remain at weekly. Thus, diurnal and day-to-day SST variability are not considered in 'exSST'.

4.4.2. Smoothed topography. Topography appears to play a key role in the formation of MCS, since many of the systems are found to be orogenic (Maddox, 1980; Velasco and Fritsch, 1987; Laing and Fritsch, 1997). Singleton and Reason (2006, 2007) showed that the topography over eastern South Africa is important for the evolution of cut-off lows. This topography

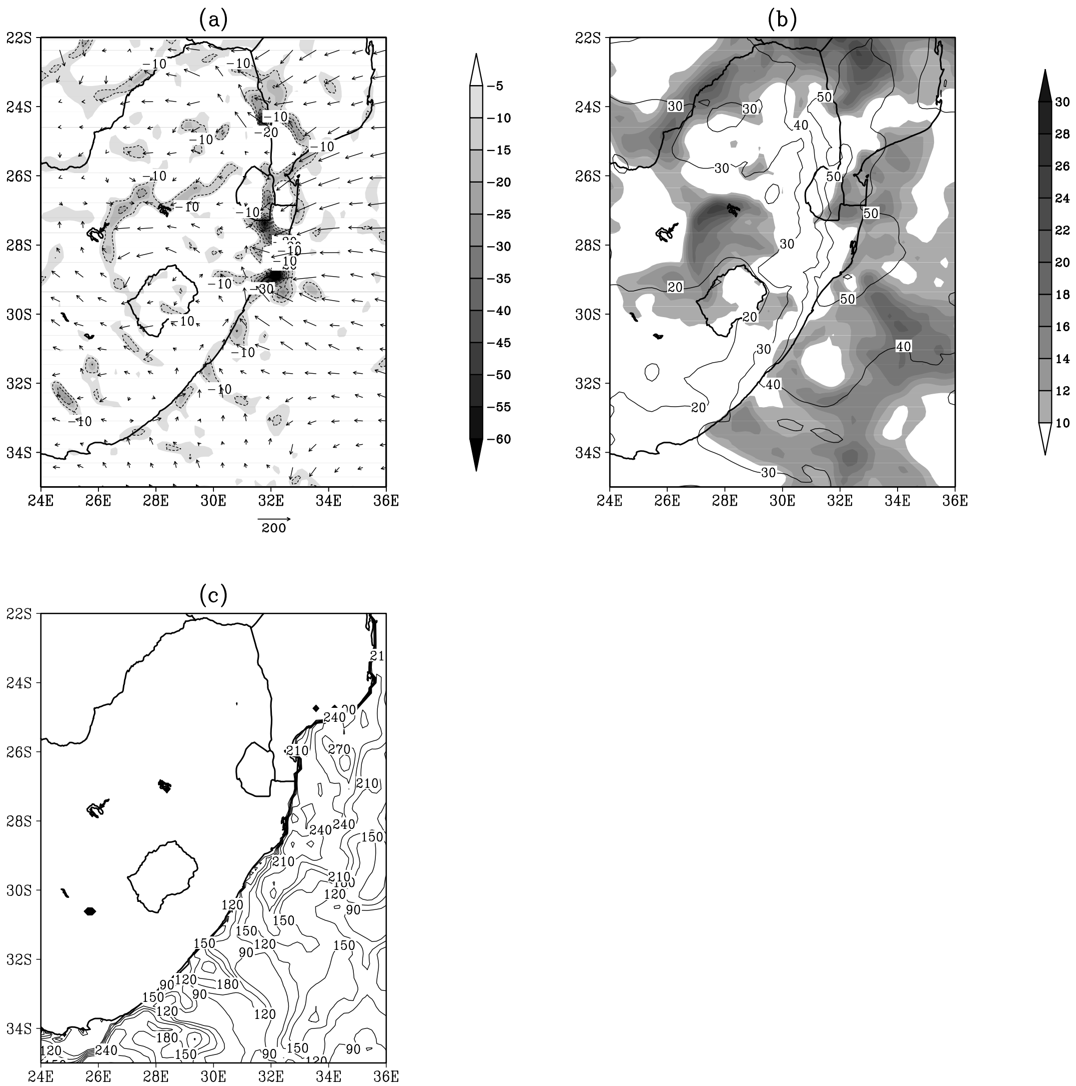

Fig. 12. Same as Fig. 9, but for the 'exSST'.

reaches altitudes over 3000m in the eastern interior and is believed to play a role in triggering MCSs (Laing and Fritsch, 1993b). In addition, the local coastal topography may play a role in promoting uplift of moist air. To test the potential role of the topography, a run in which the terrain height throughout the domain was reduced by 75% was performed (exTOPO). However, since the MRF boundary conditions contain the signature of the real topography, 'exTOPO' does not completely remove all topographic effects.

The precipitation pattern in 'exTOPO' (Fig. 8c) is considerably different to that found in the control and 'exSST' runs with most of the rainfall now confined to the northeastern parts of domain 2 (Fig. 1). In general, the magnitudes are less than the observed (Fig. 2) and control (Fig. 8a). Hourly images (not shown) revealed that most of the precipitation that took place in the extreme northeastern parts of KZN begun in the late afternoon (1600 UTC 11 February), spread northwards and continued until just after 0000 UTC in Mozambique.

The model OLR indicates that the MCS in 'exTOPO' failed to develop along the eastern escarpment. However, a convective system did develop along the far northeastern region of KZN in the late afternoon of 11 February at the time the model rainfall began. This convective system strengthened during the late afternoon and night, slowly propagating northwards into Mozambique. By the next day, it began to decay more rapidly than in the control. Thus, the strongly reduced topography in 'exTOPO' may have weakened the associated uplift so that it was insufficient to produce the heavy precipitation in KZN.

Changes in the horizontal winds from the control were apparent at lower levels, with northwesterly and westerly winds rather than southeasterlies dominating over KZN during the morning

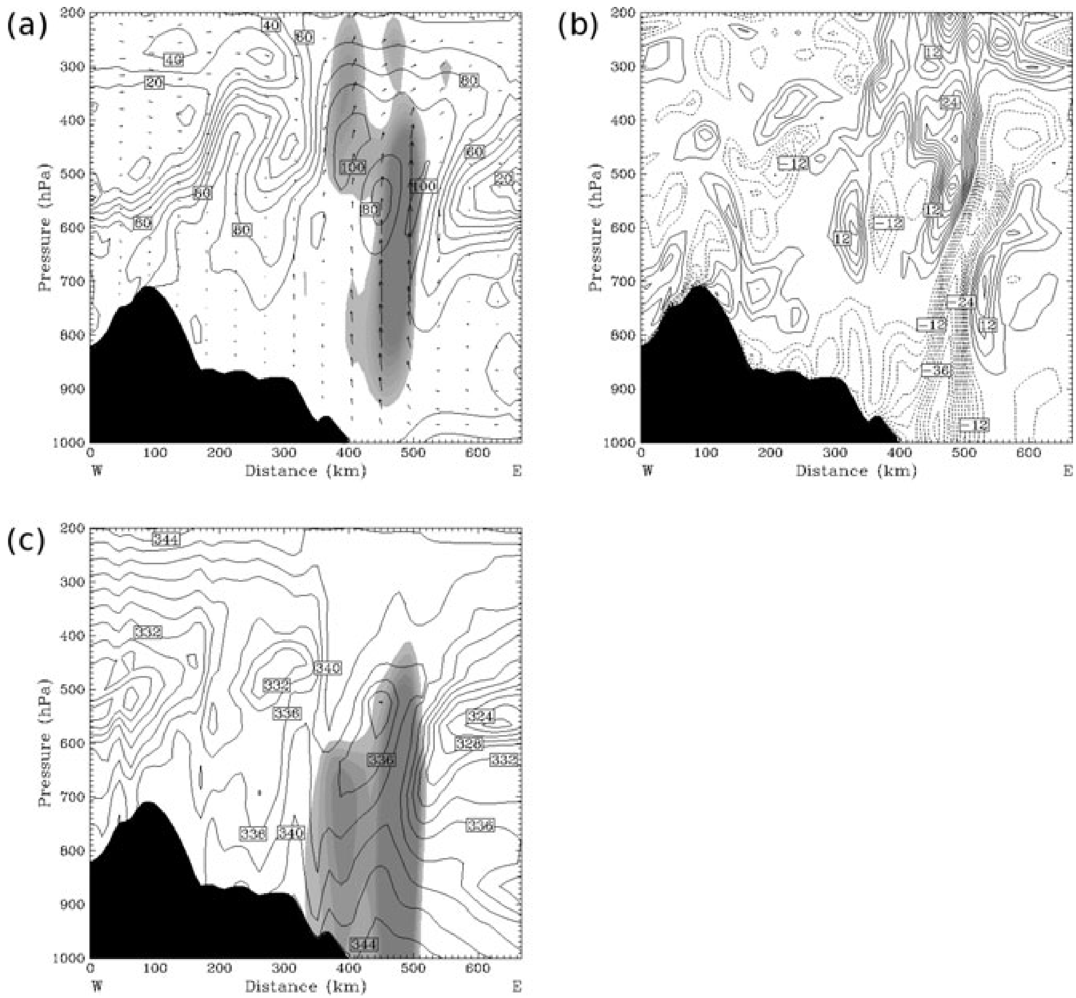

Fig. 13. Same as Fig. 11, except for 'exSST' simulation.

of 11 February. These offshore winds restricted the advection of moist marine air to the coastal regions, leading to less rainfall than the control. Even though the topography led to less surface friction, there were no significant differences in the wind strength between 'exTOPO' and the control. This result suggests that the effect of topography was more to steer the wind than to influence its magnitude.

It was evident that the moisture influx into the northeast KZN coast in 'exTOPO' was mainly from the northeast (Fig. 14a), compared to the more easterly influx found in the control run (Fig. 9a). Low-level moisture convergence over the coastal region is weaker in the 'exTOPO' run. The reduced surface latent heat flux values off the east coast (Fig. 14c) and weaker moisture flux may account for the decreased moisture convergence over the coastal region in 'exTOPO'. The precipitable water content over the coastal regions was also lower in 'exTOPO' (Fig. 14b) compared to the control run (Fig. 9b). In the control run (Fig. 9b), the contours of precipitable water content are adjacent along the eastern escarpment whereas in 'exTOPO' (Fig. 14b) they are not and there is little evidence of any linear distribution in this field.

Another feature missing from 'exTOPO' compared to the control was the offshore mesoscale anticyclone at 800–700 hPa (Fig. 14d). This feature helped increase the onshore moisture advection into coastal KZN in the control, suggesting that its absence in 'exTOPO' lead to further reduction in the rainfall.

The results suggest that the eastern escarpment played a key role in the development of the storm, since the observed MCS failed to develop over this area in 'exTOPO'. Also, the considerable underestimation of precipitation suggests that the synoptic forcing alone was not capable of producing significant precipitation for this particular event and that local orographic uplift was essential.

5. Discussion and concluding remarks

In this paper, an MCS that resulted in heavy precipitation along the northeast coast of South Africa was investigated.

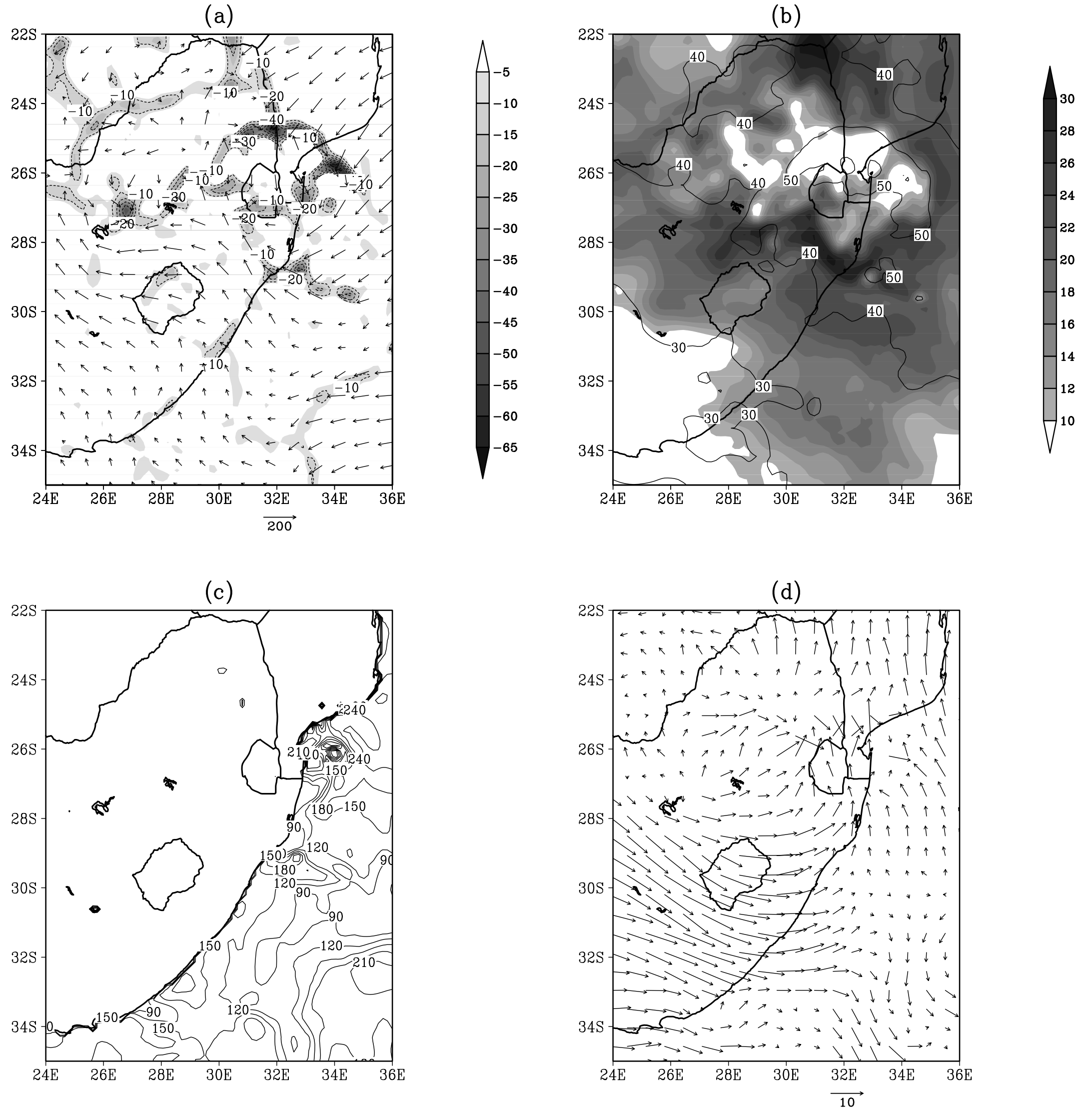

Fig. 14. Same as Fig. 9, except for the 'exTOPO' run.

South African Weather Service rainfall data indicated that this single event had a large impact on the February 2005 rainfall over northern KZN. Thus, the main emphasis here was using available observations and MM5 simulations to identify the processes that resulted in the development of the system as well as the associated heavy precipitation. Various sensitivity tests were also conducted to identify the role SST resolution and topography played in the development of this system.

Satellite imagery showed that during the early afternoon of 11 February 2005, single cell convective systems initiated over the eastern escarpment of South Africa. These individual systems then merged and developed into an MCS and strengthened during the night, resulting in heavy precipitation over parts of KZN. Medium Range Forecast model data reveal that the MCS resulted from the interaction between a ridging anticyclone, an inland surface trough and a weak westerly wave aloft. The MCS was likely to have been triggered by high diurnal surface heating and the influx of moist tropical air from the northern Agulhas Current, which was forced to rise by the eastern escarpment. Consistent with Doswell (1987) and Romero et al. (2000), the interaction of synoptic and mesoscale processes allowed the system to become large enough and persist long enough to be classified as an MCS.

The track of the MCS was similar to that indicated for MCCs over southern Africa by Laing and Fritsch (1993b). After initiating over the eastern escarpment, the MCS propagated towards the northern Agulhas Current region. Moisture influx from the northern Agulhas Current region fed and strengthened the system during the late afternoon and night of 11 February. These results reinforce the suggestion that moisture supplied from the

Agulhas Current region plays a key role in extreme precipitation events in South Africa, as identified in research on cut-off lows (e.g. Rouault et al., 2002; Singleton and Reason, 2006, 2007).

A control run of MM5 with an outer grid at 18 km and a nested grid of 6 km over the KZN region was able to capture most aspects of the MCS, although its shape was slightly different from observed and too much precipitation was produced in some regions. Mesoscale convective systems are predominately warm season events, and since parametrizations of convection may be inadequate (e.g. Kuo et al., 1996; Wang and Seaman, 1997), mesoscale models like MM5 have difficulty accurately representing precipitation. This problem may be exaggerated in places like South Africa with strong topographic, vegetation, soil moisture and SST gradients since the parametrizations developed elsewhere may not adequately represent local conditions.

The heavy precipitation along the north coast was due to sustained periods of favourable conditions for deep convection with significant onshore low-level flux of moist tropical air. However, an LLJ was absent from the control run and the MRF data, although it has been apparent in MCS cases elsewhere in the world.

To assess the role of SST forcing and local topography, a higher resolution SST (exSST) and a reduced topography (exTOPO) model run were done. The higher resolution SST data used in 'exSST' led to increased precipitation due to the presence of an easterly LLJ and enhanced moisture fluxes. In 'exTOPO', it was found that far less precipitation and reduced spatial extent occurred mainly due to the absence of orographic uplift. The influx of moisture extended further inland in the 'exTOPO' run, whereas in the other runs it was blocked by the topography and forced to rise leading to the heavy rainfall. The mesoscale anticyclone off the east coast identified in the control run failed to develop in the 'exTOPO' run. This highlights the role that the topography played in the development of this MCS event.

South Africa is frequently affected by severe weather events, but the scarcity of observations restricts our understanding of these weather systems. In addition, local modelling capacity is limited with this study representing, as far as we know, the first attempt to model a South African MCS event. Although we have only considered a single case, we believe that the model results provide further evidence of the importance of the Agulhas Current and the topography over eastern South Africa for the development of severe storms in the region. The mechanisms that result in the development of these types of storms are not completely understood nor are they well forecast, yet these systems play a large role in the weather and rainfall patterns in parts of southern Africa. An accurate assessment of the contribution of MCSs to the summer precipitation of eastern South Africa remains unknown, which further motivates for more research into these large convective systems.

6. Acknowledgments

We thank the SAWS for the station data and the synoptic charts, Swaziland Meteorology Service for rainfall data and EUMETSAT for providing the satellite images. The NCEP–NCAR data were provided by the NOAA Climate Diagnostics Centre, Boulder, USA. The NAVOCEANO SST data were obtained through the online PO:DAAC Ocean ESIP TOOL (POET) at the Physical Oceanography Distributed Active Archive Centre (PO:DAAC), NASA Jet Propulsion Laboratory, Pasadena, CA. We are also grateful for the assistance provided by K. Hansingo with the modelling. Thanks also to two anonymous reviewers whose suggestions helped improve the paper.

References

Anderson, C. J. and Arritt, R. W. 2001. Mesoscale convective systems over the United States during the 1997–98 El Niño. *Mon. Wea. Rev.* **129**, 2443–2457.

Bernardet, L. R., Grasso, L. D., Nachamkin, J. E., Finley, C. A. and Cotton, W. R. 2000. Simulating convective events using a high-resolution mesoscale model. *J. Geophys. Res.* **105**, 14963–14982.

Chen, S.-J., Wang, W., Lau, K.-H., Zhang, Q.-H. and Chung, Y.-S. 2000. Mesoscale convective systems along the Meiyu front in a numerical model. *Meteorol. Atmos. Phys.* **75**, 149–160.

Cook, C., Reason, C. J. C. and Hewitson, B. C. 2004. Wet and dry spells within particularly wet and dry summers in the South African summer rainfall region. *Clim. Res.* **26**, 17–31.

Cotton, W. R. 2000. An overview of mesoscale convective systems. Chapter 31 in *Storms vol. II* (eds. R. A. Pielke Jr. and R. A. Pielke Sr). Routledge, London, 3–25.

Cotton, W. R., Lin, M.-S., McAnelly, R. L. and Tremback, C. J. 1989. A composite model of mesoscale convective complexes. *Mon. Wea. Rev*. **117**, 765–783.

Crimp, S. J. and Masson, S. J. 1999. The extreme precipitation event of 11–16 February 1996 over South Africa. *Meteorol. Atmos. Phys.* **70**, 29–42.

D'Abreton, P. C. and Lindesay, J. A. 1993. Water vapour transport over Southern Africa during wet and dry early and later summer months. *Int. J. Climatol.* **13**, 151–170.

D'Abreton, P. C. and Lindesay, J. A. 1995. Divergent and non-divergent water vapour transport over southern Africa during wet and dry conditions. *Meteorol. Atmos. Phys*. **55**, 297–306.

Doswell, C. A. III, 1987. The distinction between large scale and mesoscale contribution to severe convection: a case study example. *Wea. Forecast.* **2**, 3–16.

Doswell, C. A. III, Brooks, H. E. and Maddox, R. A. 1996. Flash flood forecasting: an ingredients-based methodology. *Wea. Forecast.* **11**, 560–581.

Draxler, R. R. and Hess, G. D. 1997. Description of the Hysplit_4 modeling system, NOAA Technical Memorandum ERL ARL-224, December, 24 p.

Dudhia, J. 1993. A non-hydrostatic version of the Penn State-NCAR Mesoscale Model: validation tests and simulation of an Atlantic cyclone and cold front. *Mon. Wea. Rev.* **121**, 1493–1513.

Dyson, L. L. and van Heerden, J. 2001. The heavy rainfall and floods over the northeastern interior of South Africa during February 2000. *S. Afr. J. Sci.* **97**, 80–86.

García-Herrera, R., Barriopedro, D., Hernández, E., Paredes, D., Correoso, K. F. and Prieto, L. 2005. The 2001 Mesoscale Convective Systems over Iberia and the Balearic Islands. *Meteorol. Atmos. Phys*. **90**, 225–243.

Garstang, M. and Tyson, P. 2000. Mesoscale convective systems over South Africa. In: *Storms* (Chapter 38) Volume. 2 (eds. R. A. Pielke Jr. and R. A. Pielke Sr.). Routledge, London, 146–162.

Grell, G. A., Dudhia, J. and Stauffer, D. R. 1994. A description of the fifth generation Penn State/NCAR Mesoscale Model Version 5 (MM5). NCAR Technical Note NCAR/TN-398, 138 pp.

Hong, S.-Y. and Pan, H.-L. 1996. Nonlocal boundary layer vertical diffusion in a medium-range forecast model. *Mon. Wea. Rev.* **124**, 2322–2339.

Houze, R. A. Jr. 2004. Mesoscale Convective Systems. *Rev. Geophys.* **42**, 1–43, doi:10.1029/2004RG000150.

Juneng, L., Tangang, F. T. and Reason, C. J. C. 2007. Numerical case study of an extreme rainfall event during 9–11 December 2004 over the East Coast Peninsular Maylaysia. *Meteorol. Atmos. Phys*., **98**, 81–98.

Jury, M. R., Valentine, H. R. and Lutjeharms, J. R. E. 1993. Influence of the Agulhas Current on summer rainfall on the southeast coast of South Africa. *J. Appl. Meteorol*. **32**, 1282–1287.

Kalnay, E., Kanamitsu, M. and Baker, W. E. 1990. Global numerical weather prediction at the National Meteorological Center. *Bull. Am. Meteorol. Soc.* **71**, 1410–1428.

Kalnay, E., Kanamitsu, M., Kistler, R., Collins, W., Deaven, D. and co-authors. 1996. The NCEP/NCAR 40-year reanalysis project. *Bull. Am. Meteorol. Soc.* **77**, 437–471.

Kanamitsu, M. 1989. Description of the NMC global data assimilation and forecast system. *Wea. Forecast.* **4**, 334–342.

Kanamitsu, M., Alpert, J. C., Campana, K. A., Caplan, P. M., Deavan, D. G. and co-authors. 1991. Recent changes implemented into the global forecast system at NMC. *Wea. Forecast.* **6**, 425–435.

Kuo, Y.-H., Bresch, J. F., Cheng, M.–D., Kain, J., Parsons, D. B. and co-authors. 1997. Summary of a mini workshop on cumulus parameterization for mesoscale models. *Bull. Am. Meteorol. Soc.* **78**, 475–491.

Laing, A. G. and Fritsch, J. M. 1993a. Mesoscale convective complexes over the Indian Monsoon region. *J. Clim.* **6**, 911–919.

Laing, A. G. and Fritsch, J. M. 1993b. Mesoscale convective complexes in Africa. *Mon. Wea. Rev*. **121**, 2254–2263.

Laing, A. G. and Fritsch, J. M. 1997. The global population of mesoscale convective complexes. *Q. J. Roy. Meterol. Soc.* **123**, 389–405.

Laing, A. G. and Fritsch, J. M. 2000. The large-scale environments of the global populations of mesoscale convective complexes. *Mon. Wea. Rev.* **128**, 2756–2776.

Laing, A. G., Fritsch, J. M. and Negri, A. J. 1999. Contribution of mesoscale convective complexes to rainfall in Sahelian Africa: estimates from geostationary infrared and passive microwave data. *J. Appl. Meteorol.* **38**, 957–964.

Laurent, H., D'Amato, N. and Lebel, T. 1998. How important is the contribution of mesoscale convective complexes to the Sahelian rainfall. *Phys. Chem. Earth.* **23**, 629–633.

Maddox, R. A. 1980. Mesoscale convective complexes. *Bull. Am. Meteorol. Soc.* **61**, 1374–1387.

Maddox, R. A. 1983. Large-scale meteorological conditions associated with mid-latitude, mesoscale convective complexes. *Mon. Wea. Rev.* **111**, 1475–1493.

Maddox, R. A., Chappell, C. F. and Hoxit, L. R. 1979. Synoptic and meso-α-scale aspects of flash flood events. *Bull. Am. Meteorol. Soc.* **60**, 115–123.

Maddox, R. A., Howard, K. W., Bartels, D. L. and Rogers, D. M. 1986. Mesoscale convective complexes in the middle latitudes. In: *Mesoscale Meteorology and Forecasting* (ed. P.S. Ray). American Meteorology Society, 390–413.

Mathon, V., Laurent, H. and Lebel, T. 2002. Mesoscale convective system rainfall in the Sahel. *J. Appl. Meteorol.* **41**, 1081–1092.

Miller, D. and Fritsch, J. M. 1991. Mesoscale convective complexes in the western Pacific region. *Mon. Wea. Rev.* **119**, 2978–2992.

Orlanski, I. 1975. A rational subdivision of scales for atmospheric processes. *Bull. Am. Meteorol. Soc.* **56**, 527–530.

Parker, M. D. and Johnson, R. H. 2000. Organizational modes of midlatitude mesoscale convective systems. *Mon. Wea. Rev.* **128**, 3413–3436.

Reason, C. J. C. 2001. Evidence for the influence of the Agulhas Current on regional atmospheric circulation patterns. *J. Clim.* **14**, 2769–2778.

Reason, C. J. C. and Keibel, A. 2004. Tropical cyclone eline and its unusual penetration and impacts over the Southern African Mainland. *Wea. Forecast.* **19**, 789–805.

Reisner, J., Rasmussen, R. M. and Bruintjes, R. T. 1998. Explicit forecasting of supercooled liquid water in winter storms using the MM5 mesoscale model. *Q. J. Roy. Meterol. Soc.* **124**, 1071–1107.

Reynolds, R. W., Rayner, N. A., Smith, T. M., Stokes, D. C. and Wang, W. 2002. An improved in situ and satellite SST analysis for climate. *J. Clim.* **15**, 1609–1625.

Romero, R., Doswell C. A. III and Ramis, C. 2000. Mesoscale numerical study of two cases of long-lived quasi-stationary convective systems over eastern Spain. *Mon. Wea. Rev.* **128**, 3731–3751.

Rouault, M., White, S. A., Reason, C. J. C., Lutjeharms, J. R. E. and Jobard, I. 2002. Ocean-atmosphere interaction in the Agulhas Current region and a South African extreme weather event. *Wea. Forecast.* **17**, 655–669.

Rouault, M., Reason, C. J. C., Lutjeharms, J. R. E. and Beljaars, A. C. M. 2003. Underestimation of latent and sensible heat fluxes above the Agulhas Current in NCEP and ECMWF analyses. *J. Clim.* **16**, 776–782.

Singleton, A. T. and Reason, C. J. C. 2006. Numerical simulations of a severe rainfall event over the Eastern Cape coast of South Africa: sensitivity to sea surface temperature and topography. *Tellus.* **58A**, 355–367.

Singleton, A. T. and Reason, C. J. C. 2007. A numerical model study of an intense cut-off low pressure system over South Africa. *Mon. Wea. Rev.* **135**, 1128–1150.

Smith, J. A., Baeck, M. L., Zhang, Y. and Doswell C. A. III 2001. Extreme rainfall and flooding from supercell thunderstorms. *J. Hydrometeorol.* **2**, 469–489.

Tucker, D. F. and Crook, N. A. 1999. The generation of mesoscale convective systems from mountain convection. *Mon. Wea. Rev.* **127**, 1259–1273.

Tyson, P. D. and Preston-Whyte, R. A. 2000. *The Atmosphere and Weather of Southern Africa*. Oxford University press, Cape Town, 396 pp.

Velasco, I. and Fritsch, J. M. 1987. Mesoscale convective complexes in the Americas. *J. Geophys Res.* **92**, 9591–9613.

Wang, W. and Seaman, N. 1997. A comparison of convective parameterization schemes in a mesoscale model. *Mon. Wea. Rev.* **125**, 252–278.

Xie, P. and Arkin P. A. 1998. Global monthly precipitation estimates from satellite-observed outgoing longwave radiation. *J. Clim.* **11**, 137–164.

Xu, M., Bao, J.-W., Warner, T. T. and Stensrud, D. J. 2001. Effect of time size in MM5 simulations of a mesoscale convective complex. *Mon. Wea. Rev.* **129**, 502–516.